EDGE ARTICLE

Check for updates

Nonplanar structure accelerates reverse intersystem crossing of TADF emitters: nearly 40% EQE and relieved efficiency roll off†

He Liu, [ID] Yang Liu, Guohao Chen, Yuan Meng, Hao Peng, Jingsheng Miao and Chuluo Yang [ID] *

Exploring strategies to enhance reverse intersystem crossing (RISC) is of great significance to develop efficient thermally activated delayed fluorescent (TADF) molecules. In this study, we investigate the substantial impact of nonplanar structure on improving the rate of RISC (k_{RISC}). Three emitters based on spiroacridine donors are developed to evaluate this hypothesis. All molecules exhibit high photoluminescent quantum yields (PLQYs) of 96–98% due to their rigid donor and acceptor. Leveraging the synergistic effects of heavy element effect and nonplanar geometry, **S2-TRZ** exhibits an accelerated k_{RISC} of 24.2×10^5 s^{-1} compared to the 11.1×10^5 s^{-1} of **S1-TRZ**, which solely incorporates heavy atoms. Additionally, **O1-TRZ** possesses a further lower k_{RISC} of 9.42×10^5 s^{-1} because of the absence of these effects. Remarkably, owing to the high PLQYs and suitable TADF behaviors, devices based on these emitters exhibit state-of-the-art performance, including a maximum external quantum efficiency of up to 40.1% and maximum current efficiency of 124.7 cd A^{-1}. More importantly, devices utilizing **S2-TRZ** as an emitter achieve a relieved efficiency roll-off of only 7% under 1000 cd m^{-2}, in contrast to the 12% for **O1-TRZ** and 11% for **S1-TRZ**, respectively. These findings advance our fundamental understanding of TADF processes for high-performance electroluminescent devices.

1. Introduction

In the last few decades, thermally activated delayed fluorescent (TADF) emitters have emerged as highly promising materials for organic light emitting diodes (OLEDs) owing to their capability of boosting 75% triplet excitons to emit *via* reverse intersystem crossing (RISC) without the help of noble metals.[1,2] The advent of multi-resonance (MR) type emitters, characterized by narrow band emission, has positioned them as a burgeoning option aligning well with BT.2020 standards, a wide color gamut standard for the next generation of high resolution displays.[3–7] Nevertheless, MR emitters usually possess prolonged delayed fluorescence due to the large energy difference (ΔE_{ST}) between the first singlet (S$_1$) and triplet excited state (T$_1$), which impedes swift RISC processes. In response, sensitization techniques have been applied to augment the efficiency and durability of MR-emitter-based devices.[8,9] These sensitizers play a critical role in effectively recycling all excitons, thereby offering a new opportunity for leveraging conventional donor–acceptor (D–A)

type TADF compounds. Developing efficient D–A TADF emitters remains a paramount objective for realizing high performance OLEDs.

The primary task to craft an efficient TADF emitter lies in establishing a rapid RISC pathway, which necessitates a minimized ΔE_{ST} and a large spin–orbit coupling (SOC), as delineated by Fermi's golden rule.[10–12] Various structural motifs, such as twisted D–A arrangements,[13–19] through-space charge transfer (TSCT),[20–24] or multi-resonance (MR) architectures,[25–31] have successfully achieved diminutive ΔE_{ST} in pristine organic compounds. Indeed, the attainment of near-zero ΔE_{ST} has been achieved in several works, which propelled the rate of RISC (k_{RISC}) to a maximum of 10^8 s^{-1}.[32] However, conventional TADF emitters encounter an intrinsic limitation in adjusting k_{RISC} solely through ΔE_{ST} manipulation, as its minimum value is constrained to zero. To further enhance k_{RISC}, attention must be directed to optimizing SOC. Hence, heavy elements such as sulfur (S),[33–37] selenium (Se),[38–42] or noble metals[43–46] have been incorporated, which elevate the k_{RISC} value and mitigate efficiency roll-off in devices. Notably, the introduction of heavy atoms will amplify the rate of intersystem crossing (k_{ISC}) simultaneously, which will compete with the radiative decay process and potentially compromise photoluminescent quantum yield (PLQY). Therefore, despite the advantage of Se, its utilization in D–A type TADF compounds remains limited due to the inherent suppression of radiative decay caused by the

National Key Laboratory of Green and Long-Life Road Engineering in Extreme Environment (Shenzhen), Shenzhen Key Laboratory of New Information Display and Storage Materials, College of Materials Science and Engineering, Shenzhen University, 518055, Shenzhen, P. R. China. E-mail: clyang@szu.edu.cn

† Electronic supplementary information (ESI) available. See DOI: https://doi.org/10.1039/d4sc03111c

diminished overlap between frontier molecular orbitals (FMOs). Exploring alternative strategies to enhance SOC represents a promising avenue for the design of efficient TADF emitters.

Conformational twisting has long been recognized to trigger SOC in a conjugated π-electron system.[47] Nonplanar molecules usually possess a larger k_{ISC} than their planar counterparts. The spin–orbit Hamiltonian in central-field approximation could be written as[48]

$$\hat{H}_{SO} = \alpha_F{}^2 \sum_{\mu}^{N} \sum_{i}^{n} \frac{Z_\mu}{r_{i\mu}{}^3} \vec{L}_i \vec{S}_i \qquad (1)$$

where α_F represents the fine-structure constant. Z_μ denotes the effective nuclear charge at nucleus μ, and S and L are the spin and orbital angular momenta of electron i, respectively. Notably, in coplanar molecules, the SOC between π–π* orbitals yields relatively small values, whereas the 'out-of-plane' component L_z of the angular momentum operator L contributes to a non-negligible SOC. This phenomenon has been observed in polymer systems as well.[49] Recently, twisting geometry has been applied in boosting phosphorescence emission in pure organic molecules.[50–53] SOC could be effectively improved by a nonplanar structure. Additionally, You et al. reported that the nonplanar benzothiophene could accelerate k_{RISC} by reducing the ΔE_{ST}.[54] Enlightened by these valuable experiences, the

exploration of such strategies will provide a new perspective in assembling practical TADF emitters.

Herein, to validate this hypothesis, we designed and synthesized a new emitter, named 10-(4-(4,6-diphenyl-1,3,5-triazin-2-yl)phenyl)-2,7-dimethyl-10H-spiro[acridine-9,12′-benzo-[b]fluoreno[1,2-d]thiophene] (S2-TRZ), with a properly bent acridine (Fig. 1). The structurally fixed benzothiophene unit provides a substantial steric hindrance between the hydrogen atom and the acridine plane. Hence, a hooked acridine with a dihedral angle of 166° was acquired. In comparison, an isomer, 10-(4-(4,6-diphenyl-1,3,5-triazin-2-yl)phenyl)-2,7-dimethyl-10H-spiro[acridine-9,7′-benzo[b]fluoreno-[3,2-d]thio-phene] (S1-TRZ), with the same benzothiophene substitution but a more planar acridine was assembled. Additionally, the oxygen (O) equipped analogs of S1-TRZ, 10-(4-(4,6-diphenyl-1,3,5-triazin-2-yl)phenyl)-2,7-dimethyl-10H-spiro[acridine-9,7′-fluoreno[2,3-b]benzofuran] (O1-TRZ), was also forged to unveil the effect of heavy atoms. All emitters exhibit high PLQY of 96–98%, relevant with the rigid D and A units. Benefiting from the synergy of the heavy element effect and nonplanar donor structure, S2-TRZ possesses the highest k_{RISC} of 24.2 × 10^5 s^{-1}. Without the nonplanar structure, S1-TRZ with a solely heavy element effect holds a moderate k_{RISC} of 11.1 × 10^5 s^{-1}. Furthermore, lacking the nonplanar structure of the sulfur-
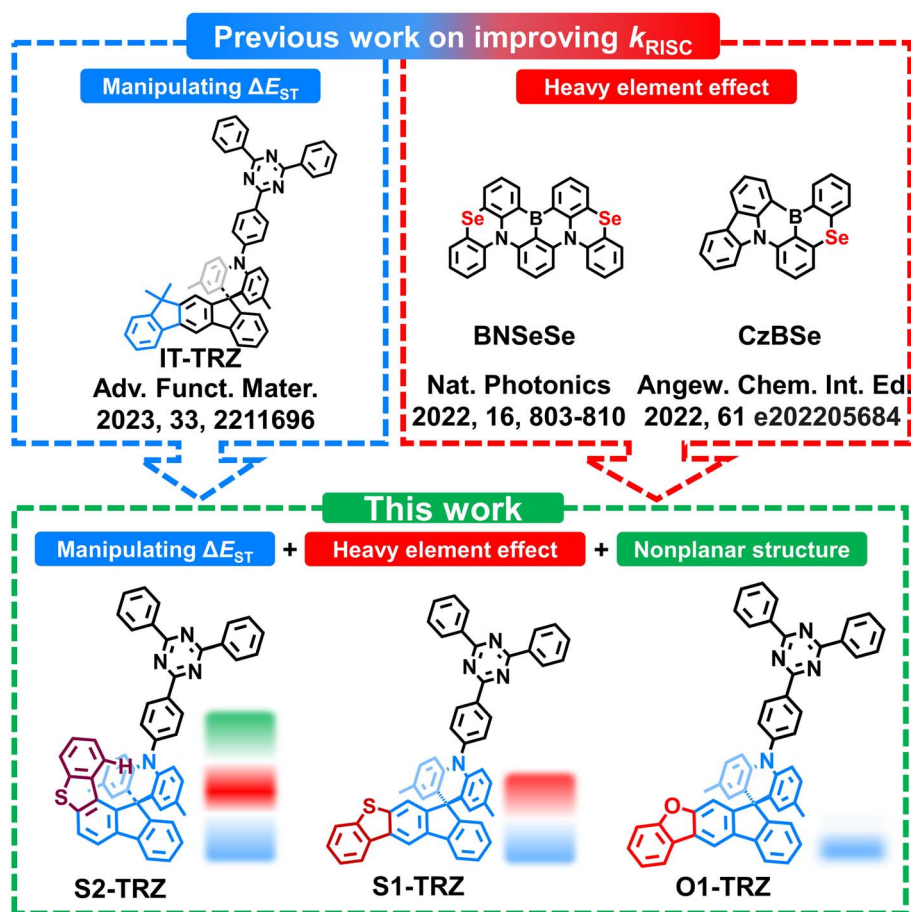

Fig. 1 Comparison of the reported work on the methods of enhancing k_{RISC}, molecular design and chemical structures of the related emitters.

containing analogs, **O1-TRZ** displays a lower k_{RISC} of 9.42×10^5 s^{-1}. Notably, electroluminescent devices based on these emitters achieved a state-of-the-art external quantum efficiency (EQE) of 39.6% for **S2-TRZ**, 39.2% for **S1-TRZ** and even 40.1% for **O1-TRZ** thanks to the exceptional molecular properties. More importantly, **S2-TRZ** enables a significantly reduced efficiency roll-off of only 7% under 1000 cd m^{-2}, outperforming both **S1-TRZ** (11%) and **O1-TRZ** (12%).

2. Results and discussion

2.1. Molecular design, synthesis and thermal properties

To validate the impact of nonplanar structures on k_{RISC}, a delicate molecular design is imperative. Nonplanar motifs within D or A groups may affect their electron-donating or -withdrawing capabilities, potentially hindering charge transfer (CT) interactions. In some cases, such motifs could lead to unfavorable conformations, such as the quasi-axial (QA) geometry, which is generally recognized to result in less efficient TADF properties. Thus, there arises a need for a building block composed of a fixed geometry with controllable modulation. Enlightened by our previous works, spiro-acridines featuring a rigid crisscross geometry could be an excellent platform to establish a model compound. To further reveal the insights for manipulating the

TADF properties, the heavy element effect is also taken into consideration. Therefore, **S2-TRZ**, **S1-TRZ** and **O1-TRZ** are designed. All the compounds were synthesized *via* conventional Buchwald–Hartwig coupling between the bromo triazine acceptor and corresponding acridine donors (Scheme S1†). The donor parts were synthesized using a previously reported one-pot reaction method in good yields.[55] All the final compounds were identified by ^{1}H NMR, ^{13}C NMR, mass spectra and elemental analysis. Excellent thermal stability is demonstrated with decomposition temperatures of 390–445 °C as evidenced by thermal gravimetric analysis (TGA) measurements (Fig. S1†). No obvious glass transition temperatures (T_gs) are detected in the range of 50–400 °C.

2.2. Theoretical simulation

To examine the properties of ground and excited states, density functional theory (DFT) and time dependent DFT (TD-DFT) were performed at the PBE0/def2svp level. As shown in Fig. 2 and S2,† **S1-TRZ** and **O1-TRZ** hold a more planar acridine unit with a dihedral angle of 173° and 177°. Conversely, **S2-TRZ** exhibits a twisted acridine with a dihedral angle of 166°, which is attributed to the spatially close hydrogen atom forming a constrained interaction with the acridine plane. These interactions could be identified using reduced density gradient

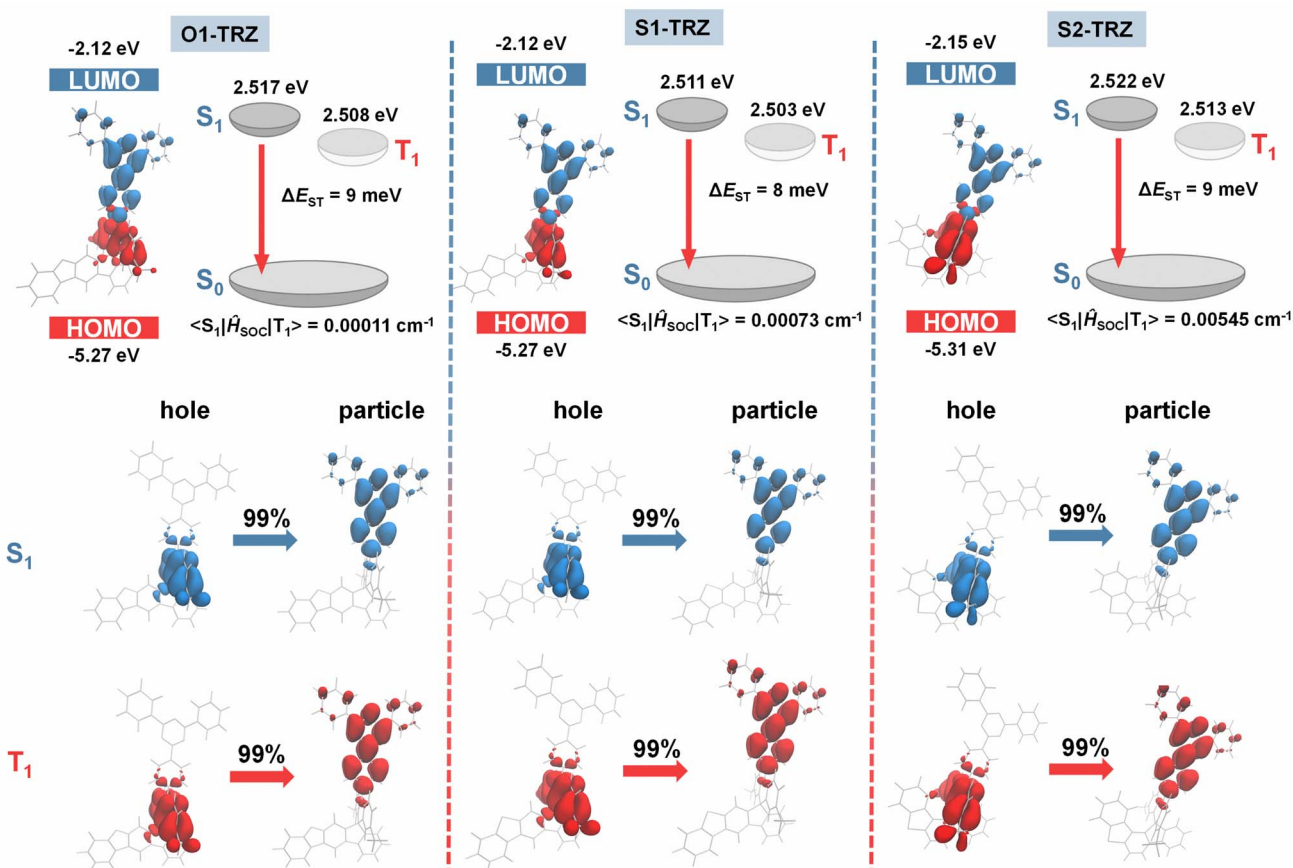**Fig. 2** Theoretical simulated distribution and energy levels of HOMO/LUMO, and NTO distribution of the particle/hole of S$_1$ and T$_1$ of **O1-TRZ**, **S1-TRZ** and **S2-TRZ** at the PBE0/def2svp level. The figures are extracted using Multiwfn.[56]

(RDG) analysis (Fig. S3†). Strong van der Waals interactions (green isosurface) and large hindrance (brown isosurface) are clearly presented. Despite the enforced bending of acridine in **S2-TRZ**, the rigid crisscross structure prevents excessive deformation, favoring a quasi-equational (QE) geometry. In contrast, both **S1-TRZ** and **O1-TRZ** exhibit predictable QE patterns. In return, all emitters show large twisting between D and A with torsion angles of 85° for **S2-TRZ**, 88° for **S1-TRZ** and 87° for **O1-TRZ**, respectively. Hence, well separated highest occupied molecular orbitals (HOMOs) and lowest unoccupied molecular orbitals (LUMOs) are established in all three molecules. LUMOs predominantly reside on triazine with similar energy levels of −2.15 eV for **S2-TRZ** and −2.12 eV for both **S1-TRZ** and **O1-TRZ**, while HOMOs mostly spread on acridine units with comparable values of −5.27 eV for both **S1-TRZ** and **O1-TRZ**, and −5.31 eV for **S2-TRZ**. All S_1 and T_1 of the three compounds exhibit CT features as revealed by the distribution of their natural transition orbitals (NTOs). Taking **S2-TRZ** for example, 'hole' NTOs localized on acridine with a small portion on the spiro-junction, while 'particle' NTOs extend over the acceptor unit. The good separation of 'hole' and 'particle' NTOs suggests small ΔE_{ST}, leading to predicted values of 9 meV for **S2-TRZ**, 8 meV for **S1-TRZ** and 9 meV for **O1-TRZ**, respectively, which may facilitate a good TADF feature. To distinguish the effect of the hooked donor, the SOC constant was calculated to be 0.00545 cm^{-1} for **S2-TRZ**, 0.00073 cm^{-1} for **S1-TRZ** and 0.00011 cm^{-1} for **O1-TRZ**, respectively (Table 1). **S1-TRZ** exhibits a slightly higher SOC than **O1-TRZ**, hinting at a weak heavy element effect. In sharp comparison, **S2-TRZ** manifests a much larger SOC value than that of **S1-TRZ**, highlighting the pronounced impact of nonplanar structure tin enhancing SOC. Theoretical simulation suggests that these emitters could exhibit efficient TADF properties, and more encouragingly, the nonplanar donor could provide an effective enhancement on SOC.

2.3. Photophysical properties

Photophysical properties were assessed in dilute toluene solution (10^{-5} M) and doped films (10 wt% in dibenzo[b,d]furan-2,8-diylbis(diphenylphosphine oxide) (PPF)). As shown in Fig. 3, the intense absorption below 320 nm is assigned to the π–π* transition. The peaks between 320 and 370 nm are attributed to the n–π* transition of the donor. Different from **O1-TRZ** and **S1-TRZ** that exhibit structural and sharp peaks, **S2-TRZ** shows a broadened absorption in this region. To gain a deep insight into this phenomenon, we have recorded the absorption of the donor unit. As shown in Fig. S5,† the n–π* transition of these emitters fits well with the absorption of their donors, which confirms that these differences are related to the donor. It is reported that the molecular absorption becomes structureless

and wide as the rigidity and planarity decrease.[57] Therefore, the broadened n–π* transition of **S2-TRZ** could probably be attributed to the decrease of the planarity and rigidity of the acridine part, which confirms the bending of the acridine as revealed by theoretical analysis. The weak peaks at 410 nm originate from the CT absorption, which suggests the tight correlation between the D and A units. Structureless blueish green emissions around 504–513 nm are observed in doped films. The energy levels of S_1 (E_{S_1})/T_1 (E_{T_1}) are calculated to be 2.72/2.67 eV for **O1-TRZ**, 2.69/2.63 eV for **S1-TRZ** and 2.73/2.67 eV for **S2-TRZ**, resulting in small ΔE_{ST}s values of 0.05, 0.06 and 0.06 eV, respectively. Moreover, Fl of these emitters was also recorded at room temperature. As shown in Fig. S4,† **O1-TRZ** and **S1-TRZ** show slightly redshifted spectra and smaller E_{S_1} of 2.66 eV for **O1-TRZ** and 2.67 eV for **S1-TRZ**, respectively. Meanwhile, **S2-TRZ** exhibits the same E_{S_1} at room temperature and 77 K, indicating **S2-TRZ** possesses less relaxation of S_1 in films. Proper TADF is corroborated via transient PL measurement, revealing distinct prompt (PF) and DF components in the decay profiles (Fig. 3b). Fitting well with two-exponential decay, lifetimes of PF (τ_p)/DF (τ_d) are deduced to be 28 ns/2.1 μs, for **O1-TRZ**, 24 ns/1.7 μs for **S1-TRZ** and 25 ns/2.3 μs for **S2-TRZ**, respectively. And the ratios of PF/DF (R_p/R_d) are 48%/52% for **O1-TRZ**, 49%/51% for **S1-TRZ** and 15%/82% for **S2-TRZ**. The higher R_p/R_d may be attributed to the higher SOC value of **S2-TRZ**, which endows it with fast ISC and RISC processes. ISC competes with radiative decay and leads to more singlet excitons converting to triplet ones and enlarges the component of DF. Additionally, all emitters show high PLQY ranging from 96 to 98%. Rate constants are further calculated using the equations provided in the ESI† and summarized in Table 2. Compared to **O1-TRZ**, **S1-TRZ** exhibits a shortened τ_p and τ_d, demonstrating higher k_r of 1.95 × 10^7 s^{-1} and k_{RISC} of 11.1 × 10^5 s^{-1}, respectively. This enhancement could be related to the introduction of S. Since S is introduced far from the D–A center, the heavy element effect could be weak as predicted by theoretical simulation. In contrast, **S2-TRZ** displays a DF-dominated TADF feature with R_p/R_d of 18%/82%, leading to significantly improved k_{RISC} of 24.2 × 10^5 s^{-1}. This substantial difference is attributed to the formation of the nonplanar donor, underscoring the significance of structural factors in TADF emitters. The HOMO energy levels of these compounds were determined using cyclic voltammetry (CV) and calculated to be 5.17 eV for **S2-TRZ**, 5.18 eV for **S1-TRZ** and 5.20 eV for **O1-TRZ**, respectively, suggesting that the nonplanar donor show minimal impact on electron donating ability. Thus, the enhanced k_{RISC} is mainly contributed by the bended structure. Photophysical analysis confirms the formation of a nonplanar donor and the accelerated RISC channels as suggested by theoretical simulation.

Table 1 Theoretical results and thermal properties of **S2-TRZ**, **S1-TRZ** and **O1-TRZ**

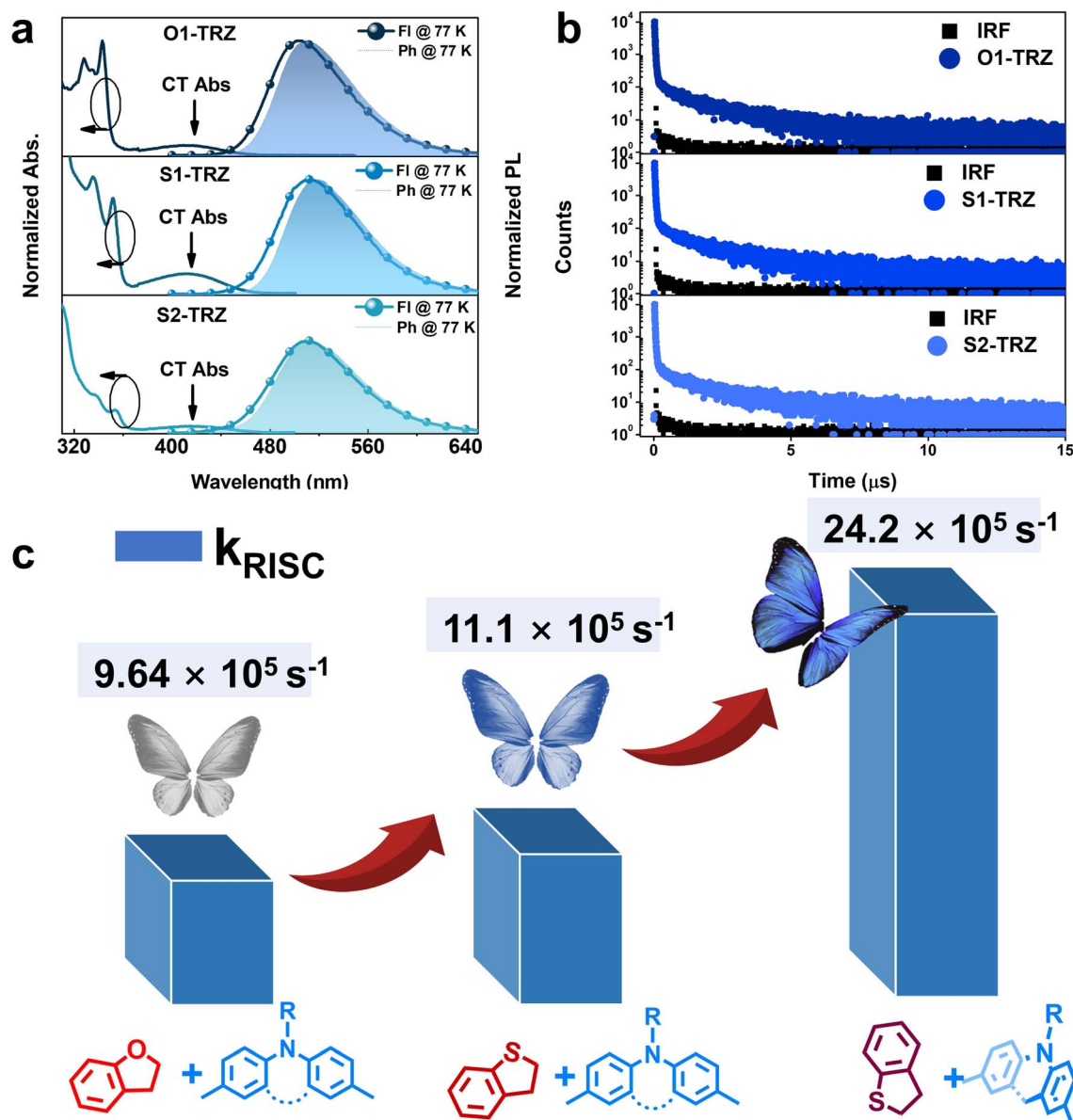| Compound	HOMO (eV)	LUMO (eV)	S_1 (eV)	T_1 (eV)	ΔE_{ST} (meV)	SOC (cm^{-1})	T_d (°C)
S2-TRZ	−5.31	−2.15	2.522	2.513	9	0.00545	445
S1-TRZ	−5.27	−2.12	2.511	2.503	8	0.00073	404
O1-TRZ	−5.27	−2.12	2.517	2.508	9	0.00011	390

Fig. 3 (a) Absorption in toluene (10^{-5} M), fluorescence (Fl) and phosphorescence (Ph) at 77 K in doped films (10 wt% in PPF) of **O1-TRZ**, **S1-TRZ** and **S2-TRZ**. (b) Transient PL decay in doped films (10 wt% in PPF) of **O1-TRZ**, **S1-TRZ** and **S2-TRZ**. (c) Comparison of k_{RISC} and structure characteristics of **O1-TRZ**, **S1-TRZ** and **S2-TRZ**.

Table 2 TADF properties of **O1-TRZ**, **S1-TRZ** and **S2-TRZ** in doped films (10 wt% in PPF)

Emitter	τ_p (ns)	τ_d (μs)	Φ_{PL} (%)	Φ_p (%)	Φ_d (%)	k_r (10^7 s^{-1})	k_{ISC} (10^7 s^{-1})	k_{RISC} (10^5 s^{-1})	k_{nr} (10^5 s^{-1})
O1-TRZ	28	2.1	98	47	51	1.69	1.87	9.64	3.45
S1-TRZ	24	1.7	96	47	49	1.95	2.09	11.1	8.03
S2-TRZ	25	2.3	97	17	80	0.70	3.27	24.2	2.15

2.4. Electroluminescent properties

To evaluate the impact of such variation on electroluminescent (EL) properties, devices based on following structures of ITO/ HATCN (5 nm)/TAPC (30 nm)/TCTA (15 nm)/mCBP (10 nm)/ PPF:emitters (10–20 wt%, 25 nm)/PPF (10 nm)/ANT-BIZ (30 nm)/Liq (2 nm)/Al were fabricated. The corresponding EL profiles are listed in Fig. 4, S6† and Table 3. Initially, these emitters were examined at a doping concentration of 10 wt% to reduce the concentration-induced quenching. Single EL emission around 504–513 nm suggests the good confinement of
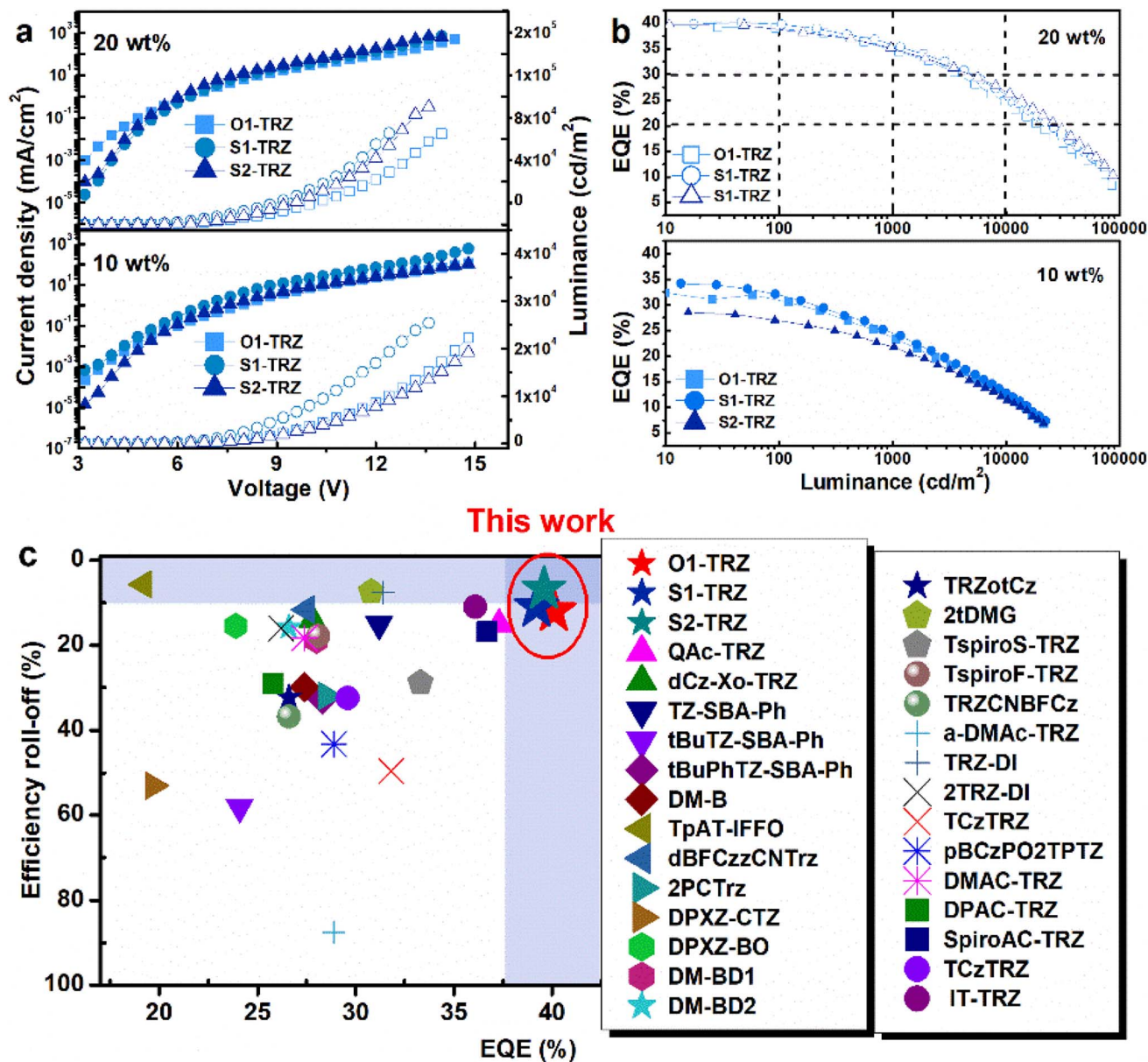
Fig. 4 (a) Current density–voltage–luminance (J–V–L) profiles; (b) EQE vs. luminance characteristics. Inset of devices based on **O1-TRZ**, **S1-TRZ** and **S2-TRZ** at 10 and 20 wt% doping concentrations. (c) Comparison of EQE and efficiency roll-off under 1000 cd m^{-2} between reported emitters.

Table 3 EL data of **O1-TRZ**, **S1-TRZ** and **S2-TRZ** based devices at different doping concentrations

Emitting layer	EL (nm)	V_{on} (V)	L_{max} (cd m^{-2})	CE^a (cd A^{-1})	EQE^a (%)	Roll-off^b (%)	CIE^c (x, y)
O1-TRZ (10 wt%):PPF	506	3.2	22 324	98.6/91.4/67.0	34.1/31.9/24.5	6/28	0.27, 0.50
S1-TRZ (10 wt%):PPF	506	3.2	25 376	95.2/88.3/66.4	33.3/31.2/23.6	6/29	0.27, 0.50
S2-TRZ (10 wt%):PPF	512	3.2	21 452	85.3/80.5/64.0	29.4/27.0/21.8	8/26	0.30, 0.53
O1-TRZ (20 wt%):PPF	515	3.2	85 230	90.4/78.2/57.8	40.1/39.8/35.3	0.7/12	0.29, 0.53
S1-TRZ (20 wt%):PPF	516	3.2	85 476	122.7/120.9/106.2	39.2/39.0/34.8	0.5/11	0.30, 0.54
S2-TRZ (20 wt%):PPF	519	3.2	110 267	124.7/124.0/115.3	39.6/39.5/36.9	0.2/7	0.31, 0.55

^{a} Maximum values at 100/1000 cd m^{-2}. ^{b} Efficiency roll-off under 100/1000 cd m^{-2}. ^{c} CIE coordinates under 6 V.

excitons. All devices exhibit turn-on voltages of 3.2 V and high luminance exceeding 21 000 cd m^{-2}. Maximum EQEs (EQE$_{max}$s) of over 29.4% are achieved with the highest value of 34.1% in

the **O1-TRZ** based device. Compared with **O1-TRZ**, the lower EQE$_{max}$ of the **S1-TRZ** based device may be attributed to its lower PLQY. And the low EQE$_{max}$ in the **S2-TRZ** based device

could result from its low k_r. Further probing the efficiency roll-off offers similar values of 6–8% under 100 cd m^{-2} and 26–29% under 1000 cd m^{-2}, which are relatively large. The electron-withdrawing nature of PPF as the host matrix may have led to carrier imbalances in the emissive layer. Therefore, devices with concentration optimization were evaluated at 20 wt%. Remarkably, all devices achieve improved performance with a significantly enhanced luminance of 85 000 to 110 000 cd m^{-2} and increased EQE$_{max}$ values of 39.6% for **S2-TRZ**, 39.2% for **S1-TRZ** and 40.1% for **O1-TRZ**. These results demonstrate their sufficient exciton utilization at a doping concentration of 20 wt%. Besides high PLQY and efficient TADF features, the excellent EL performances also benefit from high molecular horizontal dipole ratios, which will enhance the out-coupling efficiency. The p-polarized PL spectra are shown in Fig. S7,† suggesting that these emitters exhibit horizontal dipole ratios in the range of 80–97%. Such high values will greatly enhance the out-coupling efficiency and boost the EQE to nearly 40%. Notably, efficiency roll-off is substantially reduced with negligible roll-offs under 100 cd m^{-2}. At a higher luminance level, **O1-TRZ** and **S1-TRZ** achieve similar roll-off of 12% and 11% under 1000 cd m^{-2}, respectively, while **S2-TRZ** shows a small value of only 7%. Compared to **O1-TRZ**, **S1-TRZ** with slightly larger k_{RISC} produces a comparable roll-off. **S2-TRZ** features a higher k_{RISC} than **S1-TRZ**, experiencing a much gentler roll-off. The synergistic effect of the heavy element effect and nonplanar structure contributes to a significant enhancement of the RISC channel, facilitating the rapid consumption of excitons.

3. Conclusion

In conclusion, we have disclosed the great impact of nonplanar structure on accelerating the RISC channel in TADF emitters. By combining cross-coupled spiroacridine and structurally fixed compulsory hindrance, **S2-TRZ** with a properly hooked acridine is successfully established. Analogs of **S1-TRZ** composed of a coplanar acridine and **O1-TRZ** with an O atom are designed to distinguish the effect of the nonplanar geometry and heavy element effect, respectively. All compounds exhibit high PLQYs of 96–98% and small ΔE_{ST}s of 8–9 meV, indicating excellent TADF behaviors. **S2-TRZ** with both heavy atoms and a nonplanar structure shows the highest k_{RISC} of 24.2×10^5 s^{-1}, whereas **S1-TRZ** possesses a lower k_{RISC} of 11.1×10^5 s^{-1} due to the absence of a nonplanar acridine. Lacking these benefits, **O1-TRZ** displays the lowest k_{RISC} of 9.64×10^5 s^{-1}. Encouragingly, all emitters exhibit amazing EL performance with EQE$_{max}$ of 39.6% for **S2-TRZ**, 39.2% for **S1-TRZ** and even 40.1% for **O1-TRZ**, respectively, alongside ultra-high luminance of up to 100 000 cd m^{-2}. More importantly, **S2-TRZ** with a large value of k_{RISC} exhibits the lowest roll-off of 7% under 1000 cd m^{-2}, indicating the importance of the nonplanar structure in enhancing RISC for excellent EL performance. Overall, the effectiveness of nonplanar geometry in accelerating the RISC channel has been theoretically and experimentally validated. This strategy represents a valuable alternative to manipulating SOC besides the heavy atom effect. This work provides guidance for designing practical TADF emitters.

Data availability

All data supporting the findings of this study are presented in the article and ESI.† Additional data are available from the corresponding author upon reasonable request.

Author contributions

H. Liu designed the study. C. L. Yang supervised the project. Y. Liu and G. H. Chen performed the experiments. Y. Meng, H. Peng and J. S. Miao collected and analyzed the data. All the authors discussed the results and co-wrote the manuscript.

Conflicts of interest

There are no conflicts to declare.

Acknowledgements

References

1 H. Uoyama, K. Goushi, K. Shizu, H. Nomura and C. Adachi, *Nature*, 2012, **492**, 234–238.

2 Q. Zhang, B. Li, S. Huang, H. Nomura, H. Tanaka and C. Adachi, *Nat. Photonics*, 2014, **8**, 326–332.

3 Y. Kondo, K. Yoshiura, S. Kitera, H. Nishi, S. Oda, H. Gotoh, Y. Sasada, M. Yanai and T. Hatakeyama, *Nat. Photonics*, 2019, **13**, 678–682.

4 M. Yang, I. S. Park and T. Yasuda, *J. Am. Chem. Soc.*, 2020, **142**, 19468–19472.

5 J. Liu, Y. Zhu, T. Tsuboi, C. Deng, W. Lou, D. Wang, T. Liu and Q. Zhang, *Nat. Commun.*, 2022, **13**, 4876.

6 Y. Zou, J. H. Hu, M. X. Yu, J. S. Miao, Z. Y. Xie, Y. T. Qiu, X. S. Cao and C. L. Yang, *Adv. Mater.*, 2022, **34**, 2201442.

7 X.-C. Fan, K. Wang, Y.-Z. Shi, Y.-C. Cheng, Y.-T. Lee, J. Yu, X.-K. Chen, C. Adachi and X.-H. Zhang, *Nat. Photonics*, 2023, **17**, 280–285.

8 S. O. Jeon, K. H. Lee, J. S. Kim, S.-G. Ihn, Y. S. Chung, J. W. Kim, H. Lee, S. Kim, H. Choi and J. Y. Lee, *Nat. Photonics*, 2021, **15**, 208–215.

9 C.-Y. Chan, M. Tanaka, Y.-T. Lee, Y.-W. Wong, H. Nakanotani, T. Hatakeyama and C. Adachi, *Nat. Photonics*, 2021, **15**, 203–207.

10 G. W. Robinson and R. P. Frosch, *J. Chem. Phys.*, 1963, **38**, 1187–1203.

11 V. Lawetz, G. Orlandi and W. Siebrand, *J. Chem. Phys.*, 1972, **56**, 4058–4072.

12 P. K. Samanta, D. Kim, V. Coropceanu and J. L. Bredas, *J. Am. Chem. Soc.*, 2017, **139**, 4042–4051.

13 Y. Wada, H. Nakagawa, S. Matsumoto, Y. Wakisaka and H. Kaji, *Nat. Photonics*, 2020, **14**, 643–649.

14 W. Zeng, T. Zhou, W. Ning, C. Zhong, J. He, S. Gong, G. Xie and C. Yang, *Adv. Mater.*, 2019, **31**, e1901404.

15 T. A. Lin, T. Chatterjee, W. L. Tsai, W. K. Lee, M. J. Wu, M. Jiao, K. C. Pan, C. L. Yi, C. L. Chung, K. T. Wong and C. C. Wu, *Adv. Mater.*, 2016, **28**, 6976–6983.

16 R. Pei, Y. Xu, J. Miao, H. Peng, Z. Chen, C. Zhou, H. Liu and C. Yang, *Angew. Chem., Int. Ed.*, 2023, **135**, 202217080.

17 W. Li, B. Li, X. Cai, L. Gan, Z. Xu, W. Li, K. Liu, D. Chen and S. J. Su, *Angew. Chem., Int. Ed.*, 2019, **58**, 11301–11305.

18 L.-S. Cui, A. Gillett, S.-F. Zhang, H. Ye, Y. Liu, X.-K. Chen, Z.-S. Lin, E. Evans, W. Myers, T. Ronson, H. Nakanotani, S. Reineke, J. Bredas, C. Adachi and R. Friend, *Nat. Photonics*, 2020, **12**, 636–642.

19 W. Han, J. Liu, C. Ran, Z. Huang, G. Gao, J. You and Z. Bin, *Angew. Chem., Int. Ed.*, 2023, **62**, e202312297.

20 T. Huang, Q. Wang, G. Meng, L. Duan and D. Zhang, *Angew. Chem., Int. Ed.*, 2022, **61**, e202200059.

21 X. J. Zheng, R. J. Huang, C. Zhong, G. H. Xie, W. M. Ning, M. L. Huang, F. Ni, F. B. Dias and C. L. Yang, *Adv. Sci.*, 2020, **7**, 1902087.

22 C. Wu, W. Liu, K. Li, G. Cheng, J. Xiong, T. Teng, C. M. Che and C. Yang, *Angew. Chem., Int. Ed.*, 2021, **60**, 3994–3998.

23 X. Tang, L. S. Cui, H. C. Li, A. J. Gillett, F. Auras, Y. K. Qu, C. Zhong, S. T. E. Jones, Z. Q. Jiang, R. H. Friend and L. S. Liao, *Nat. Mater.*, 2020, **19**, 1332–1338.

24 S. Luo, J. Wang, N. Li, X. F. Song, X. Wan, K. Li and C. Yang, *Angew. Chem., Int. Ed.*, 2023, **62**, e202310943.

25 Y. Xu, C. Li, Z. Li, Q. Wang, X. Cai, J. Wei and Y. Wang, *Angew. Chem., Int. Ed.*, 2020, **59**, 17442–17446.

26 Z. Ye, H. Wu, Y. Xu, T. Hua, G. Chen, Z. Chen, X. Yin, M. Huang, K. Xu, X. Song, Z. Huang, X. Lv, J. Miao, X. Cao and C. Yang, *Adv. Mater.*, 2023, **36**, 2308314.

27 Y. Zhang, G. Li, L. Wang, T. Huang, J. Wei, G. Meng, X. Wang, X. Zeng, D. Zhang and L. Duan, *Angew. Chem., Int. Ed.*, 2022, **61**, e202202380.

28 F. Liu, Z. Cheng, Y. Jiang, L. Gao, H. Liu, H. Liu, Z. Feng, P. Lu and W. Yang, *Angew. Chem., Int. Ed.*, 2022, **61**, e202116927.

29 Y. Hu, M. Huang, H. Liu, J. Miao and C. Yang, *Angew. Chem., Int. Ed.*, 2023, **62**, e202312666.

30 P. Jiang, J. Miao, X. Cao, H. Xia, K. Pan, T. Hua, X. Lv, Z. Huang, Y. Zou and C. Yang, *Adv. Mater.*, 2021, e2106954.

31 T. Hatakeyama, K. Shiren, K. Nakajima, S. Nomura, S. Nakatsuka, K. Kinoshita, J. Ni, Y. Ono and T. Ikuta, *Adv. Mater.*, 2016, **28**, 2777–2781.

32 N. Aizawa, A. Matsumoto and T. Yasuda, *Sci. Adv.*, 2021, **7**, eabe5769.

33 R. Braveenth, H. Lee, J. D. Park, K. J. Yang, S. J. Hwang, K. R. Naveen, R. Lampande and J. H. Kwon, *Adv. Funct. Mater.*, 2021, 2105805.

34 X. Xiong, Y.-C. Cheng, K. Wang, J. Yu and X.-H. Zhang, *Mater. Chem. Front.*, 2023, **7**, 929–936.

35 T. Hua, L. Zhan, N. Li, Z. Huang, X. Cao, Z. Xiao, S. Gong, C. Zhou, C. Zhong and C. Yang, *Chem. Eng. J.*, 2021, **426**, 131169.

36 I. S. Park, K. Matsuo, N. Aizawa and T. Yasuda, *Adv. Funct. Mater.*, 2018, **28**, 1802031.

37 F. Chen, L. Zhao, X. Wang, Q. Yang, W. Li, H. Tian, S. Shao, L. Wang, X. Jing and F. Wang, *Sci. China: Chem.*, 2021, **64**, 547–551.

38 Y. X. Hu, J. Miao, T. Hua, Z. Huang, Y. Qi, Y. Zou, Y. Qiu, H. Xia, H. Liu, X. Cao and C. Yang, *Nat. Photonics*, 2022, **16**, 803–810.

39 X. S. Cao, K. Pan, J. S. Miao, X. L. Lv, Z. Y. Huang, F. Ni, X. J. Yin, Y. X. Wei and C. L. Yang, *J. Am. Chem. Soc.*, 2022, **144**, 22976–22984.

40 J. Jin, S. Wang, H. Jiang, L. Wang and W. Y. Wong, *Adv. Opt. Mater.*, 2024, 2302354.

41 Y. X. Hu, J. S. Miao, C. Zhong, Y. Zeng, S. L. Gong, X. S. Cao, X. Zhou, Y. Gu and C. L. Yang, *Angew. Chem., Int. Ed.*, 2023, **62**, e202302478.

42 I. S. Park, H. Min and T. Yasuda, *Angew. Chem., Int. Ed.*, 2022, **61**, e202205684.

43 D. Di, A. Romanov, L. Yang, J. M. Richter, J. P. H. Rivett, S. Jones, T. H. Thomas, M. A. Jalebi, R. H. Friend, M. Bochmann and D. Credgington, *Science*, 2017, **356**, 159–163.

44 J. Yang, X. Feng, N. Li, J. Li, X. Song, M. Li, G. Cui, J. Zhang, C. Jiang, C. Yang and K. Li, *Sci. Adv.*, 2023, **9**, eadh0198.

45 X. Feng, J. G. Yang, J. Miao, C. Zhong, X. Yin, N. Li, C. Wu, Q. Zhang, Y. Chen, K. Li and C. Yang, *Angew. Chem., Int. Ed.*, 2022, **61**, e202209451.

46 J. J. Wang, N. Q. Li, C. Zhong, J. S. Miao, Z. Y. Huang, M. X. Yu, Y. X. Hu, S. Luo, Y. Zou, K. Li and C. L. Yang, *Adv. Mater.*, 2023, **35**, 2208378.

47 K. Schmidt, S. Brovelli, V. Coropceanu, D. Beljonne, J. Cornil, C. Bazzini, T. Caronna, R. Tubino, F. Meinardi, Z. Shuai and J.-L. Brédas, *J. Phys. Chem. A*, 2004, **111**, 10490–10499.

48 S. K. Lower and M. A. El-Sayed, *Chem. Rev.*, 1966, **66**, 199–241.

49 D. Beljonne, Z. Shuai, G. Pourtois and J. L. Bredas, *J. Phys. Chem. A*, 2001, **105**, 3899–3907.

50 H. Liu, Y. Gao, J. Cao, T. Li, Y. Wen, Y. Ge, L. Zhang, G. Pan, T. Zhou and B. Yang, *Mater. Chem. Front.*, 2018, **2**, 1853–1858.

51 G. Pan, Z. Yang, H. Liu, Y. Wen, X. Zhang, Y. Shen, C. Zhou, S.-T. Zhang and B. Yang, *J. Phys. Chem. Lett.*, 2022, **13**, 1563–1570.

52 X. Yang, S. Wang, K. Sun, H. Liu, M. Ma, S. T. Zhang and B. Yang, *Angew. Chem., Int. Ed.*, 2023, **62**, e202306475.

53 X. Cai, Z. Qiao, M. Li, X. Wu, Y. He, X. Jiang, Y. Cao and S. J. Su, *Angew. Chem., Int. Ed.*, 2019, **58**, 13522–13531.

54 Y. Shi, G. Yang, B. Shen, Y. Yang, L. Yan, F. Yang, J. Liu, X. Liao, P. Yu, Z. Bin and J. You, *J. Am. Chem. Soc.*, 2021, **143**, 21066–21076.

55 H. Liu, Z. W. Liu, G. G. Li, H. N. Huang, C. J. Zhou, Z. M. Wang and C. L. Yang, *Angew. Chem., Int. Ed.*, 2021, **60**, 12376–12380.

56 T. Lu and F. Chen, *J. Comput. Chem.*, 2012, **33**, 580–592.

57 N. I. Nijegorodov and W. S. Downey, *J. Phys. Chem.*, 1994, **98**, 5639–5643.